# Stair Climbing Using a Compliant Modular Robot

Sri Harsha Turlapati[1], Mihir Shah[1], S Phani Teja[1], Avinash Siravuru[2], Suril V. Shah[1], Madhava Krishna K[1]

***Abstract*— Stair Climbing is a key functionality desired for robots deployed in Urban Search and Rescue (USAR) scenarios. A novel compliant modular robot was proposed earlier to climb steep and big obstacles. This work extends the functionality of this robot to ascend and descend stairs of dimensions that are also typical of an urban setting. Stair Climbing is realized by equipping the robot's link joints with optimally designed passive spring pairs that resist clockwise and counter clockwise moments generated by the ground during the climbing motion. This 3-module robot is only propelled by wheel actuators. Desirable stair climbing configurations are estimated a-priori and used to obtain the optimal stiffness for springs. Extensive numerical simulation results over different stair configurations are shown. The numerical simulations are corroborated by experimentation using the prototype and its performance is tabulated for different types of surfaces.**

## I. Introduction

For any robot that is deployed in an urban setting, the ability to successfully ascend and descend stairs is indispensable. Several kinds of robots that are deployed in urban settings, such as Bipedal Robots [1], [2], [3], Wheel-Legged systems [4], [5], Segway Robots [6], [7], Tracked [8], [9], [10] and Modular Robots [11], boast of this feature. [12] also provides an interesting work for unstructured and uneven terrain. Conventionally, stairs have been treated as an uneven terrain and thus most robots that demonstrate stair climbing are tracked or legged. Though tracks and legs have better traversing ability on an uneven terrain, they are still slower than wheeled robots with the same actuator system. Hence there is an added advantage for articulated wheeled robots for stair climbing. However, except for a few notable ones like Shrimp [13] and an optimally designed Rocker-Bogie [14], there is a dearth of literature on articulated wheeled robots ascending and descending stairs. Even in the above two cases, only stair ascent is shown.

In the current work, we attempt to bridge this gap with our proposed compliant modular robot, shown in Fig. 1. The compliant modular robot consists of three modules, each consisting of a link and a wheel-pair. The link-joints are fitted with passively compliant elements (springs) to limit the robot's flexibility to desired levels and efficiently traverse on uneven terrain. Our previous work [15] has already shown that the robot can climb heights up to three times its wheel diameter. The robot developed was very light-weight, made of simple and easily replaceable off-the-shelf parts thus helping in quickly prototyping and deploying such robots in larger numbers and lowering the time taken for search and rescue by facilitating a large scale parallelization of the process.

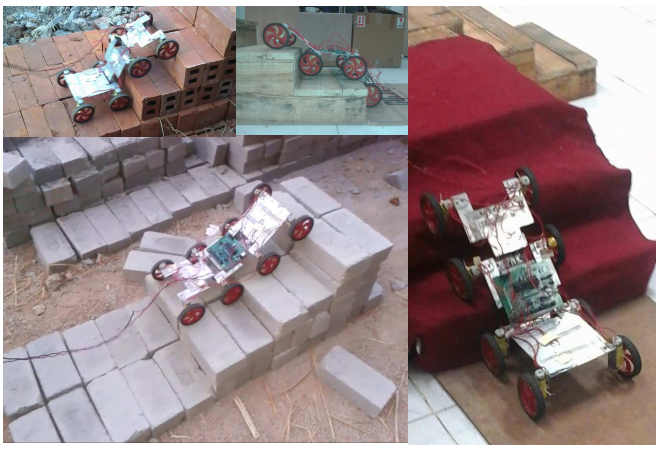

Fig. 1: Compliant modular robot prototype

It was shown in our previous works [15], [16] that compliance helps in redistributing normal forces acting on the wheels and thereby allowing them to generate higher traction force while climbing. Hence, wheels tend to slip less and traverse better on uneven terrains. Note however that, the choice of spring stiffness has an impact on the robot's traversing ability. This paper discusses in sufficient detail how this optimal spring stiffness is determined for effectively ascending stairs. The key novelty of this work is the usage of a spring-pair at every link joint as opposed to a single spring [15].

During stair climbing, both clockwise and counter clockwise moments act at the robot's joints, in a periodic manner, while tracing the contour of the steps. During ascent, an optimally designed torsional spring-pair is used at every link-joint to store the energy generated from bending along the step, and effectively re-use it while straightening, to push the robot upwards. During descent, the spring-pair helps in absorbing the kinetic energy generated while falling off the step riser and using it to move faster on the tread. This clearly demonstrates the utility of compliance in enabling a wheeled robot to swiftly navigate on uneven terrain. Extensive numerical simulation results are presented to validate this climbing behaviour. The robot is able to ascend and descend a wide variety of steps whose slopes range from $\approx 20^\circ$ to $35^\circ$. Clearly, it is a broad spectrum of slopes in terms of the variations in both riser and tread lengths. This is experimentally presented as well.

Sri Harsha Turlapati, Mihir Shah, S Phani Teja, Suril V. Shah and K Madhava Krishna are with the Robotics Research Lab, IIIT-Hyderabad, TS 500032, India. Corresponding Author: harsha.turlapati at research.iiit.ac.in

Avinash Siravuru is with the Department of Mechanical Engineering, Carnegie Mellon University, Pittsburgh, PA 15213, USA.

The paper is organized as follows. In Section II, the stair climbing ability of the modular robot is analysed and the need for a spring-pair as opposed to a single spring at the joints, is justified elaborately. Also, a method to estimate robot configurations is introduced. Section III outlines the quasi static analysis of the robot and the optimization procedure to estimate the joint stiffness. The numerical simulation results of ascending and descending stairs are shown and analysed in Section IV. Section V presents the experiments carried out for ascending and descending of stairs on various types of surfaces. Finally, conclusions and the scope for future work are discussed in Section VI.

## II. Stair Climbing Analysis for a Compliant Modular Robot

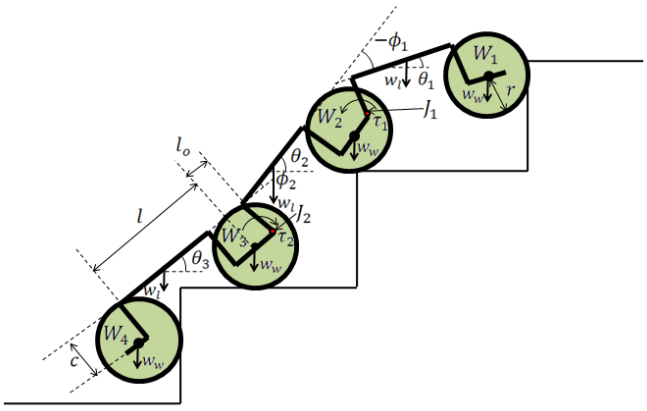


Fig. 2: Schematic of the 3-module robot

Since the robot is active wheel - passive joint type, it is necessary to ensure that the wheels don't slip while traversing and the robot maintains forward motion. A schematic of this 3-module robot is shown in Fig. 2 and its model parameters are provided in Table I. The link joints are denoted by $J_1$ and $J_2$, whereas wheel joints are denoted by $W_1$, $W_2$, $W_3$ and $W_4$. $\theta_i$ denotes the absolute angle of module $i$ while $\phi_i$ denotes the relative angle between modules $i$ and $i+1$ measured from module $i+1$. The moment acting at joint $J_i$ is denoted by $\tau_i$.

TABLE I: Model Parameters of the Compliant Module Robot

| Symbols | Quantity | Values |
|---|---|---|
| $l$ | Link Length | $0.15\ m$ |
| $b$ | Link Breadth | $0.1\ m$ |
| $r$ | Wheel Radius | $0.045\ m$ |
| $l_0$ | Wheel Joint and Link Joint Offset | $0.03\ m$ |
| $c$ | Link Height from Wheel Center | $0.0626\ m$ |
| $\tau_{wmax}$ | Stall Torque of Wheel Motors | $0.6\ Nm$ |
| $m_w$ | Mass of Each Wheel | $0.1\ Kg$ |
| $m_l$ | Mass of Each Link | $0.4\ Kg$ |

### A. Challenges in Stair Climbing

In our previous work [15], it was shown that adding an optimally designed compliant joint at $J_1$ enabled the robot to climb obstacles up to three times the wheel diameter. This robot with only one spring at $J_1$, was tested on a staircase of pitch angle $25°$. Here, pitch angle (hereafter denoted by $\alpha$) is defined as $tan^{-1}(h/t)$, where $h$ and $t$ denote the lengths of riser and tread respectively, as shown in Fig. 3. The spring aids Wheel-1 in climbing the riser of the first step. Once on the top, as Wheel-2 grazes the tread and Wheel-1 begins climbing the riser of the second step, the robot gets into an undesirable configuration where $\phi_1$, the relative angle between Module-1 and Module-2, decreases significantly causing Wheel-2 to lift off the ground. This results in a stationary configuration ($which\ occurs\ just\ after\ the\ configuration\ shown\ in$ Fig. 3) that stalls forward motion along the stairs. We propose

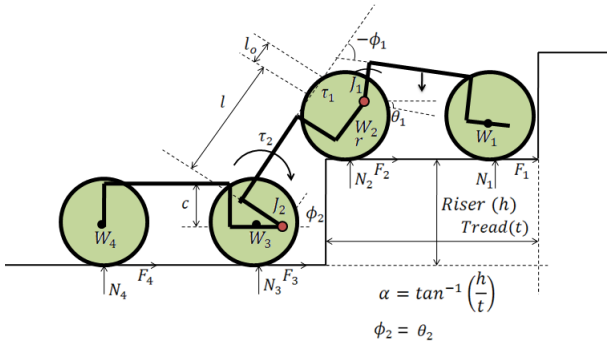


Fig. 3: The robot getting stuck while ascending stairs with only one spring at $J_1$

to overcome this situation by using another spring at $J_1$ that resists clockwise moments. Similar requirement will arise at $J_2$ also as the robot ascends higher. Ideally, when an articulated robot is used to climb stairs, it is desired that the high degree of freedom enables the robot to naturally deform along the contour of the stairs. Cases arise during stair ascent and descent where wheels lose contact resulting in stationary configurations as discussed above.

We propose to avoid this by using two springs at each joint. $k_1$ and $k_2$ are stiffness values for Joints $J_1$ and $J_2$, respectively. For the sake of convenience, we denote the stiffness of springs opposing counter-clockwise and clockwise moments for joint $i$ as $k_i^+$ and $k_i^-$, respectively. The optimal stiffness for both springs can be determined by estimating the range of clockwise and counter-clockwise moments acting on the robot during stair climbing. The robot typically traverses at speeds of $0.25$ m s$^{-1}$ on flat ground. Therefore, it is observed that the inertial forces are minimal and a quasi-static analysis could be used to study robot's climbing motion.

In order to get better insight into the problem discussed above, expressions for normal forces of Wheel-1 and Wheel-2 with and without springs are derived from the static equilibrium equations for moments at $J_1$ and $J_2$, respectively,

i.e.,

$$\sum M_{J_1} = 0 \qquad \sum M_{J_2} = 0$$

Without the springs at the Joints $J_1$ and $J_2$ the normal forces $N_1$, $N_2$ are obtained as :

$$N_1 = \frac{2w_w l cos\theta_1 + w_l(\frac{l}{2}cos\theta_1) + csin\theta_1}{D_1} \tag{1}$$

$$N_2 = \frac{A + BN_1}{D_2} \tag{2}$$

$where,$
$D_1 = 2lcos\theta_1 + 2\mu(r + lsin\theta_1)$

$A = w_l(\frac{3l}{2}cos\theta_2 + l_o cos\theta_2 - csin\theta_2) + 2w_w l_o cos\theta_2$

$B = 2(l + l_o)(\mu sin\theta_2 - cos\theta_2)$

$D_2 = 2lcos\theta_2 - 2\mu(lsin\theta_2 - r)$

With the addition of springs $k_1^-$ and $k_2^+$, the normal forces $N_1'$ and $N_2'$ are obtained as follows.

$$N_1^{'} = N_1 + \frac{k_1^- \phi_1}{D_1} \tag{3}$$

$$N_2^{'} = N_2 + \frac{1}{D_2}\left[k_2^+\phi_2 - k_1^-\phi_1(1 - \frac{B}{D_1})\right] \tag{4}$$

Rearranging the above equations, we have,

$$D_1(N_1^{'} - N_1) = k_1^-\phi_1 \tag{5}$$

$$D_2(N_2^{'} - N_2) = \left[k_2^+\phi_2 - k_1^-\phi_1(1 - \frac{B}{D_1})\right] \tag{6}$$

The values of $D_1$ and $D_2$ are found to be positive for all the progressive stages (Iterations as mentioned in Fig. 4) of the robot from the instance Wheel-2 has climbed the riser of the first step till it reaches the configuration shown in Fig. 3. Note that, given the design of the compliant joint, $k_i^+$ comes into play when $\phi_i$ is positive and $k_i^-$ when $\phi_i$ is negative. It is evident from (5) that the difference between $N_1^{'}$ and $N_1$ is $\frac{1}{D_1}[k_1^-\phi_1]$. Similarly from (6), the difference between the normal forces $N_2^{'}$ and $N_2$ at $W_2$ is given by $\frac{1}{D_2}\left[k_2^+\phi_2 - k_1^-\phi_1(1 - \frac{B}{D_1})\right]$. Therefore one may always design springs, $k_1^-$ and $k_2^+$ to impose $N_1^{'} < N_1$ and $N_2 < N_2^{'}$, since this avoids the stationary configuration discussed above. This condition is encompassed in the objective function considered in subsection III B. The profiles for the normal forces with springs (stiffness values taken from those obtained in subsection III B) and without springs are plotted in Fig. 4. These were calculated using (1), (2), (3) and (4).

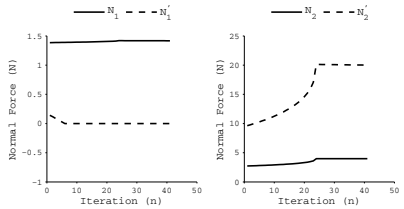


Fig. 4: Normal Force for (a) Wheel-1 and (b) Wheel-2 without (Block line) and with (Dashed line) $k_1^-$ and $k_2^+$

### B. Robot Configuration Estimation

Quasi static analysis of the robot plays an important role in finding the optimal spring stiffness values. Therefore, in order to perform the analysis, the stair climbing motion of the robot needs to be divided into discrete phases and the static forces must be estimated at each configuration. This is a non-trivial problem for highly articulated systems like the modular robot. For a given position of Wheel-1 center on the staircase, the subsequent modules can have more than one possible configuration. This problem can be alleviated by formulating an objective and choosing configurations that best adhere to it. The objective in the case of stair climbing is to always maintain contact with the step, wherever possible. In this subsection, a systematic procedure is devised to derive such configurations.

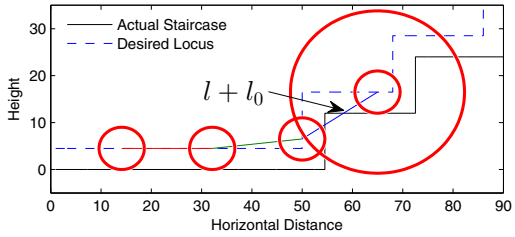


Fig. 5: Demonstration of finding Wheel center of Wheel-2 when given the wheel center of Wheel-1.

Note that, sufficient ground clearance $(c + r)$ is provided to ensure the links never collide with the ground [15]. Next we draw locus of Wheel-1 center in such a way so that the wheel always touches the ground while climbing the stairs. Now it is straightforward to observe that Wheel-2 center will be approximately at the intersection of the circle of radius $l + l_0$ (drawn from Wheel-1 center) and the locus of Wheel-1. An illustration of this process is shown Fig. 5. For an $n$-modular robot, the slope of module $i$ and subsequently its absolute angle can be determined from the center points of Wheels $i$ and $i + 1$.

The stair contour is discretized into $z$ steps. For every point $j \in [1, z]$ that Wheel-1 center passes while stair climbing, the corresponding absolutes angles ($\theta$'s) for all the modules are obtained. Furthermore, relative joint angles ($\phi$'s) can be obtained using $\phi_i = \theta_i - \theta_{i+1}$. In this manner, the desired

configurations of the robot for stair climbing are derived. This procedure is simple and very effective in determining the robot configurations on any known terrain model. In the next section, the quasi-static analysis of the robot is carried out and the optimal joint stiffness is estimated.

## III. Compliant Joint Design

It was proposed earlier, in Section II, that two springs with complementary action are required at every joint for successful stair climbing. However, it must be noted that the spring-pair fitted to every joint will not act simultaneously. The net direction of the resultant moment, generated due to static forces, changes periodically while climbing stairs. Accordingly, the springs are activated through compression alternatively. Therefore, to estimate the spring stiffness of all the springs fitted to the robot, the quasi static analysis has to be divided into phases. In each phase, the springs that are in action are identified and their optimal stiffness values are calculated. It will be shown in the next subsection that three phases are sufficient to determine the optimal stiffness values of two pairs of springs, one fitted at Joints $J_1$ and another at $J_2$. This is because, the same phases repeat when the robot climbs more number of steps.

### A. Quasi Static Analysis of the Robot

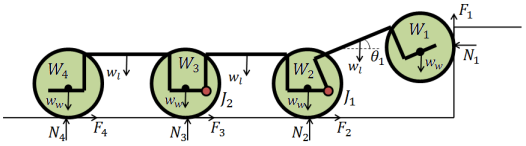


Fig. 6: Phase-1: $0 \leq \phi_1 \leq \phi_1^{max}$ and $\phi_2 = 0$

In Phase-1, only spring at $J_1$ that resists counter-clockwise moments will act. Hence the stiffness value of $k_1^+$ is calculated from this phase. The static equilibrium equations for Phase-1 are the same as in [15] and are not reported here for brevity. The forces acting on the robot are depicted in Fig. 6. Here, $F_i$ and $N_i$ denote traction and normal forces at Wheel-$i$, respectively.

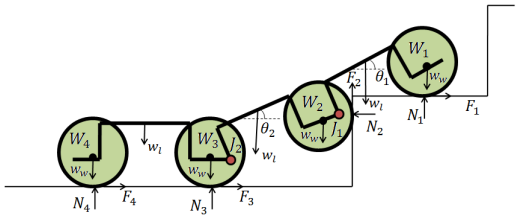


Fig. 7: Phase-2: $\phi_1^{min} \leq \phi_1 \leq \phi_1^{max}$ and $0 \leq \phi_2 \leq \phi_2^{max}$

In Phase-2, as shown in Fig. 7, both clockwise moments and counter-clockwise moments need to be resisted at $J_1$ as the Wheel-2 climbs the riser and $\phi_1$ decreases from a positive value to a negative value. The counter-clockwise moments are resisted at $J_2$. The stiffness value of $k_1^-$ has been calculated from this phase.

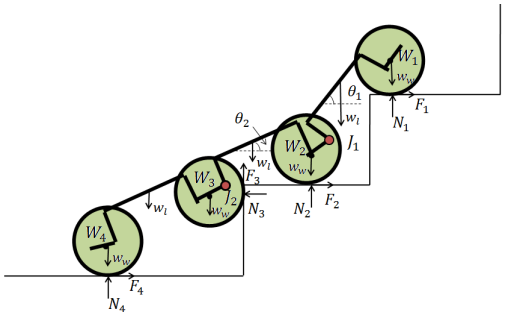


Fig. 8: Phase-3: $0 \leq \phi_1 \leq \phi_1^{max}$ and $\phi_2^{min} \leq \phi_2 \leq \phi_2^{max}$

Finally, in Phase-3 as shown in Fig. 8, counter-clockwise moments are resisted at both $J_1$ and $J_2$. Additionally, clockwise moments are also resisted at $J_2$ as $\phi_2$ decreases from a positive value to a negative value. Hence the stiffness values of $k_2^+$ and $k_2^-$ are calculated.

The static equilibrium equations for Phase-2 and Phase-3 are shown in Appendix. In the next section estimation of optimal spring stiffness values is showcased.

### B. Optimization of Link Joint Moments

The objective function for the optimization is taken as the maximization of the normal forces at each of the wheels. This is justified by the fact that with increase in normal force, the traction force increases and helps in better climbing. The optimization is carried out for all climbing phases shown in Figs. 6, 7 and 8. The objective function is given below:

$$\text{Maximize} \quad {N_{1,j}}^2 + {N_{2,j}}^2 + {N_{3,j}}^2 + {N_{4,j}}^2 \ \forall \ j \in [1, z_p]$$

subject to

$$\mathbf{F}_j \leq min(\tau_{\mathbf{wmax}}/r, \mu \mathbf{N}_j)$$

$$\mathbf{A}_p \mathbf{x}_p = \mathbf{B}_p$$

where, $\boldsymbol{\tau} = [\tau_1 \ \tau_2]^T$, $\mathbf{F} = [F_1 \ F_2 \ F_3 \ F_4]^T$, $\mathbf{N} = [N_1 \ N_2 \ N_3 \ N_4]^T$, and the vector of design variable $\mathbf{x}_p = [{\mathbf{F}_j}^T \ {\mathbf{N}_j}^T \ {\boldsymbol{\tau}_j}^T]^T \ \forall \ j \in [1,z_p]$. Moreover, $F_i$'s and $N_i$'s denote traction and normal forces acting at wheel-pair $i$, and $\tau_i$'s denote the moments at the link joints as mentioned before. $\tau_{\mathbf{wmax}}$ denotes the saturation torque of the wheel motors, and $\mathbf{A}_p \mathbf{x}_p = \mathbf{B}_p$ denotes the static equilibrium equations for Phase-$p$, where $\mathbf{x}_p$ is the design variable and $\mathbf{A}_p$ is its coefficient matrix. $\mathbf{B}_p$ refers to the terms of inertial moment left out in the quasi static equations shown in the Appendix. Finally, $z_p$ denotes the number of steps for which the optimization is carried out in Phase-$p$. The above optimization process gives the optimal $\boldsymbol{\tau}$ values (solved over an unbounded region of $\boldsymbol{\tau}$) required at the two joints to maintain static equilibrium without slipping while maximizing the normal reaction of each of the wheel, among other solutions. The moment ($\tau_i$) versus joint angle profiles are shown in Fig. 9.

Note that, most of them are almost linear and the spring constant can be estimated by a simple linear interpolation of

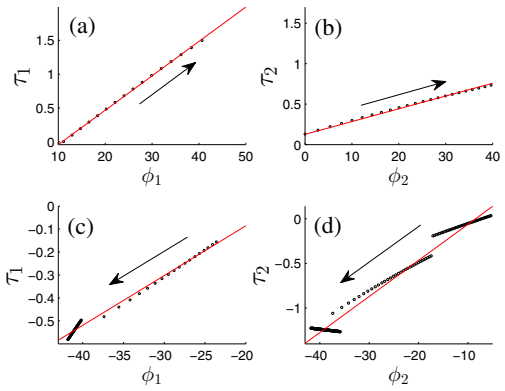


Fig. 9: Moment Profile ($\tau_i$) obtained at : (a) $J_{i=1}$ for increasing profile of Joint angle $\phi_1$ for $k_1^+$ (from Phase-1) (b) $J_{i=2}$ for increasing profile of Joint angle $\phi_2$ for $k_2^+$ (from Phase-3) (c) $J_{i=1}$ for decreasing profile of Joint angle $\phi_1$ for $k_1^-$ (from Phase-2) (d) $J_{i=2}$ for decreasing profile of Joint angle $\phi_2$ for $k_2^-$ (from Phase-3)

the data, as shown below.

$$\underset{\mathbf{k}}{\text{Minimize}} \quad \sum_{j=1}^{p} (\boldsymbol{\tau}^j - \mathbf{k}\boldsymbol{\phi}^j)^2 \tag{7}$$

Here, $\mathbf{k} = diag(k_1, k_2)$, where $k_1$ and $k_2$ are stiffness values for Joints $J_1$ and $J_2$, respectively, as discussed in subsection II A and $\boldsymbol{\phi} = [\phi_1 \ \phi_2]^T$. Following the quasi static analysis in the previous subsection, we obtain the stiffness $k_1^+$ for the spring resisting counter-clockwise moments at $J_1$ from Phase-1. The spring stiffness value obtained from Phase-2 is $k_1^-$ for joint $J_1$. This is obtained by fitting a curve (shown in red) to account for the moment profile required for joint angles during ascent. Finally, we obtain $k_2^+$ and $k_2^-$ values from Phase-3. From the linear interpolation of the joint moment profiles, the following stiffness values were obtained for springs at Joints $J_1$ and $J_2$:

$$k_1^+ = 0.0506\ Nm/deg \quad \& \quad k_1^- = 0.0216\ Nm/deg,$$
$$k_2^+ = 0.0161\ Nm/deg \quad \& \quad k_2^- = 0.0267\ Nm/deg.$$

## IV. Numerical Simulation of Stair Climbing

After determining the optimal stiffness values for the springs, the compliant modular robot was numerically simulated in MD ADAMS, a multibody dynamics simulator, to analyse robot's stair climbing ability. Six different stair case dimensions were chosen from a pitch angle range of $\approx 20°$ to $35°$ to demonstrate wide range of robot's climbing capability. The riser-to-tread ratio of $\approx 0.59$ is considered optimal which corresponds to a pitch angle of about $30°$ [17]. Figs. 11 and 12 show snapshots of numerical simulations of the robot successfully ascending and descending stairs whose pitch angles are $33.42°$ and $26.56°$ respectively. It is worth noting that the robot was able to successfully descend the stairs, despite the external deforming moments at the joint being greater than the balancing spring moments. Note that, the linear interpolation used for spring design underestimated the desired joint moments in this case. This clearly demonstrates the robustness of this design.

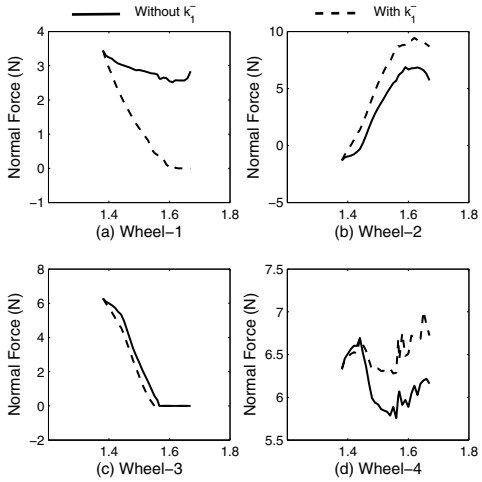


Fig. 10: Graphs depicting the Normal Forces at all the wheel-pairs for cases with spring of stiffness $k_1^-$ (dashed) and without it (solid)

As discussed in Section II, the second spring at $J_1$ (of $k_1^-$ stiffness) plays a key role in ascending stairs. This can be clearly verified from the normal force plots shown in Fig. 10. The solid line depicts the normal forces without $k_1^-$ for all the wheels for the phases before and during the time when the Wheel-1 is climbing the riser of the second step. Similarly, the dashed line depicts the normal forces when $k_1^-$ is used at $J_1$. It can be seen that Wheel-2 has a higher normal force value when the second spring is used. This further validates the theoretical results showcased in Fig. 4 i.e., $N_1^{'} < N_1$ and $N_2 < N_2^{'}$.

Additionally, a reactive moment acts on Module-3 that tends to lift Wheel-3 off the ground and redistribute the normal force to Wheel-4 as can be noted from the Fig. 10 (c)-(d). Note that, once Wheel-3 hits the riser of the step and starts climbing, it is Wheel-2 and Wheel-4 that need to provide traction in the horizontal direction and move the robot forward. The second spring clearly aids in this process.

Additional simulations were carried out on stairs with pitch angles ranging from $\approx 20°$ to $35°$, and the robot's climbing behaviour was analysed. The average speeds and mean slip ratios of the robot for all stair dimensions, are listed in Table. II. It was observed that on a flat ground, the compliant modular robot maintains a speeds of upto $0.25$ m $s^{-1}$. From the six simulations, it was recorded that the robot maintained an average speed of $0.147$ m $s^{-1}$ during ascent and $0.223$ m $s^{-1}$ during descent. They are within a close range of its flat terrain speed. It is also worth noting that, in spite of obtaining the spring stiffness from a quasi-static analysis, the springs of these values were able to balance out inertial forces whenever they were generated. The average slip ratio of all the wheels was computed to be in the range of $0.10$ to $0.30$ which is reasonably low for stair ascent and

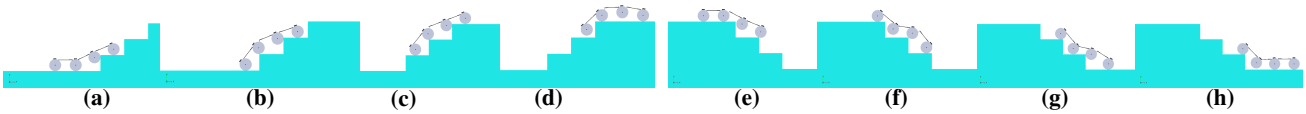


Fig. 11: Stages(a)-(h) Numerical Simulation of the robot on stair dimensions as riser length of $12cm$ and tread length as $18cm$

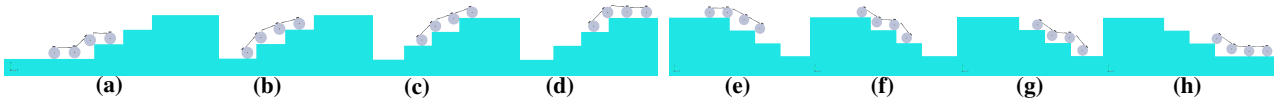


Fig. 12: Stages(a)-(h) Numerical Simulation of the robot on stair dimensions as riser length of $11cm$ and tread length as $22cm$

descent.

## V. EXPERIMENTATION

In order to validate the theoretical and numerical simulation results on the effectiveness of using compliance at Joints $J_1$ and $J_2$ proposed in the earlier sections, several experiments have been carried out on a real prototype of the robot.

The springs were fabricated as per the optimal stiffness values determined in Section III B. Accordingly, the spring's inner and outer diameter were designed to be as 0.007m and 0.0086m respectively and is made of music wire with number of coils as 3.5. The mechanical structure of the robot is same as [15] according to the parameters mentioned in Table. I. The spring assembly is depicted in Fig. 13. An open loop control was implemented as the objective of the experiments was to show the effectiveness of compliance at joints during stair climbing.

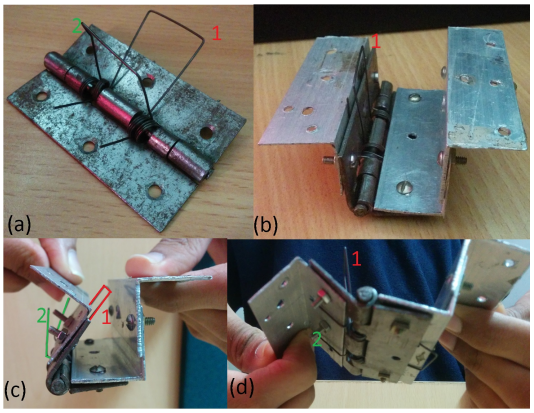


Fig. 13: The Spring Assembly - $k^+$ is labeled as (1) and $k^-$ is labeled as (2) : (a) Spring loaded hinge, (b) Joint with mounts for the robot, (c) $k^+$ in action and (d) $k^-$ in action

As mentioned in subsection II A, our robot in [15] equipped with one spring $k_1^+$ at Joint $J_1$ was unable to climb the riser of the second step with stair dimensions of riser length as $11cm$ and tread length as $22cm$. This has been demonstrated both numerically and experimentally as seen in Fig. 14.

In order to overcome this problem, springs in both clockwise and anti-clockwise direction at Joints $J_1$ and $J_2$ were added, as discussed in subsection II A. Figs. 15 (a)-(g) depict that the robot was able to climb stairs with the same dimensions when springs $k_1^-$ and $k_2^+$ are added to Joints $J_1$ and $J_2$ respectively. This experiment validates the efficacy of spring pair in redistributing normal forces as demonstrated in Fig. 10.

Additionally, the robot was tested on various stair dimensions mentioned in Table. II with step pitch angle $(\alpha)$ varying from $\approx 20°$ to $35°$. Figs. 15, 16, 17 and 18 show the experiments conducted on various stair dimensions using different surfaces like wood, concrete, ceramic bricks and carpet. This proves the robustness of the proposed robot under small variations in stair dimension and/or coefficient of friction.

It was also observed that the same stiffness values of the springs could help in descending stairs even though they were not specifically optimized for descending. Figs. 17 (e)-(f) and Figs. 18 (e)-(h) show the descending of the robot experimentally. Note that in stair climbing, the combined action of the springs in different configurations makes the robot behave differently. While descending, if the counter clockwise moment resisting spring were too stiff, the robot would have folded on itself. There were no such cases of toppling observed even with pitch angles as steep as $\approx 35°$. The maximum height the robot could climb experimentally was found to be $12cm$.

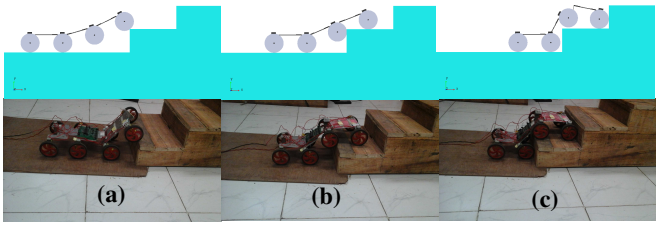


Fig. 14: Numerical Simulation and Experimentation on robot with only one spring($k_1^+$) at Joint $J_1$

TABLE II: Performance of the Robot during Stair Climbing

| Sr.No. | Step Pitch Angle (deg) | Tread length (mm) | Riser length (mm) | Avg. Speed(m $s^{-1}$) | | Mean Slip Ratio | | Material |
|---|---|---|---|---|---|---|---|---|
| | | | | Ascent | Descent | Ascent | Descent | |
| 1 | 23.74 | 180 | 80 | 0.1507 | 0.2194 | 0.1976 | -0.1683 | Wood |
| 2 | 26.56 | 220 | 110 | 0.1422 | 0.2268 | 0.2428 | -0.2077 | Wood |
| 3 | 33.42 | 180 | 120 | 0.1456 | 0.2252 | 0.2247 | -0.1991 | Wood |
| 4 | 28.36 | 220 | 120 | 0.1387 | 0.2322 | 0.2614 | -0.2364 | Concrete |
| 5 | 19.79 | 220 | 80 | 0.1608 | 0.2142 | 0.1438 | -0.1406 | Red Brick(smooth) |
| 6 | 34.21 | 160 | 110 | 0.1466 | 0.2225 | 0.2194 | -0.1848 | Red Brick(smooth) |

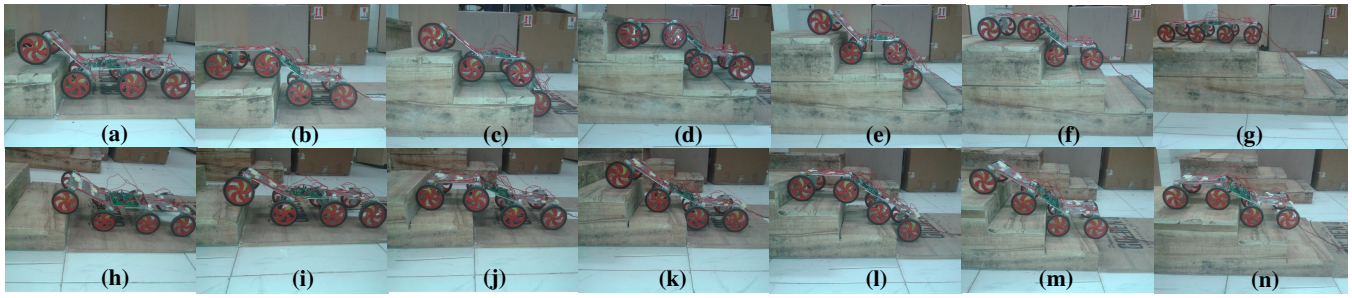


Fig. 15: Stages (a)-(g)The robot is ascending on stairs with dimensions as $11cm$ riser height and $22cm$ tread width and Stages(h)-(n) as $8cm$ riser height and $18cm$ tread width

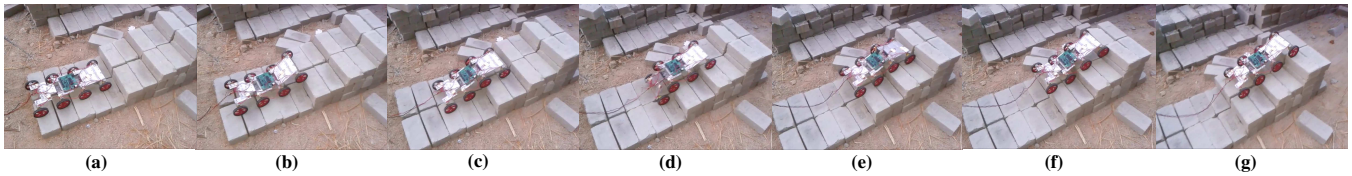


Fig. 16: Stages (a)-(g)The robot is ascending on concrete stairs with dimensions as $12cm$ riser height and $22cm$ tread width

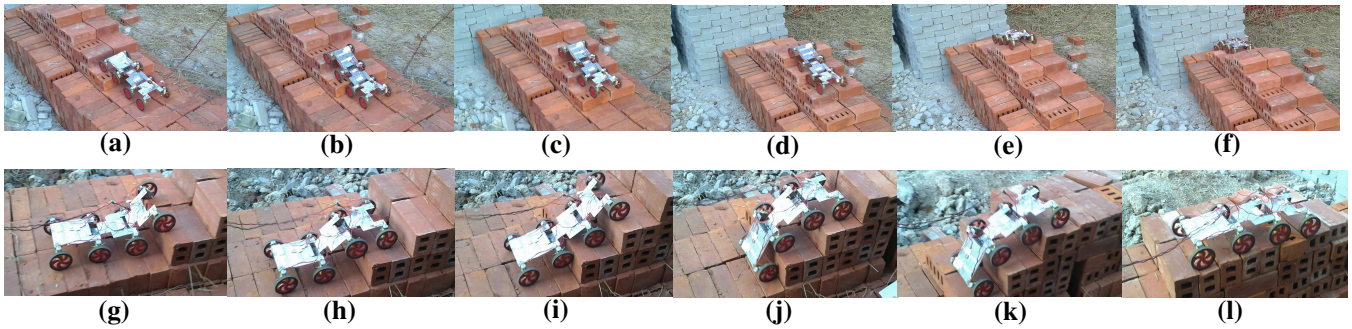


Fig. 17: Stages (a)-(f)The robot is ascending and descending on redbrick stairs with dimensions as $8cm$ riser height and $22cm$ tread width and Stages (g)-(l) with dimensions as $11cm$ riser height and $16cm$ tread width

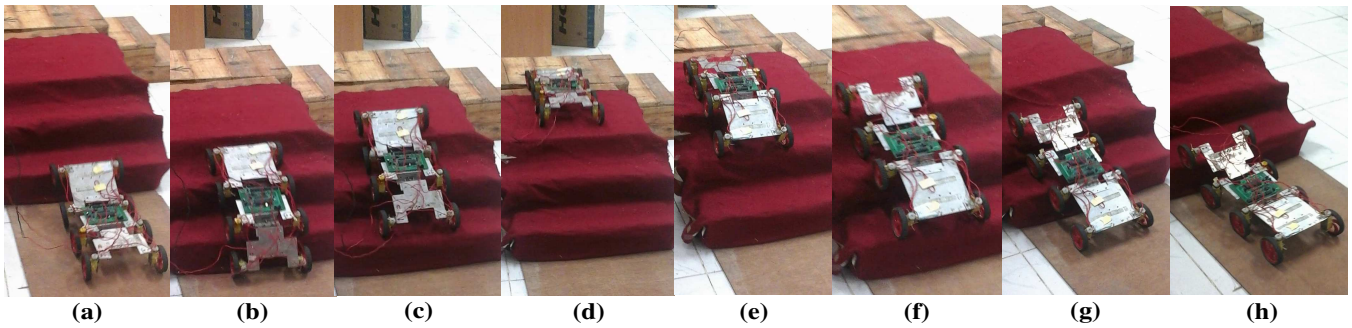


Fig. 18: Stages (a)-(d)The robot is ascending and in (e)-(h) descending on carpet stairs with dimensions as $12cm$ riser height and $18cm$ tread width

## VI. Conclusions and Future Work

In this work, we proposed that the compliant 3-module robot was able to ascend and descend stairs of various pitch angles by the addition of spring-pairs at link Joints $J_1$ and $J_2$. The role of springs in helping the robot successfully climb stairs has been explained in detail. Numerical simulations have been carried out on various stair dimensions. Moreover, experimentation was performed on the prototype to validate the theory and simulations. The robot was able to climb stairs with pitch angle ranging from $\approx 20^\circ$ to $35^\circ$. Additionally, the robot was also tested on various surfaces and its performance was tabulated.

Future work would focus on analysing performance of our robot on stairs with an overhang. Furthermore, we wish to develop joints whose stiffness can be actively varied, to further enhance the robot's traversing ability.

## References


[1] Philipp Michel, Joel Chestnutt, Satoshi Kagami, Koichi Nishiwaki, James Kuffner, and Takeo Kanade. Gpu-accelerated real-time 3d tracking for humanoid locomotion and stair climbing. In *IEEE/RSJ International Conference on Intelligent Robots and Systems (IROS)*, 2007.

[2] Chenglong Fu and Ken Chen. Gait synthesis and sensory control of stair climbing for a humanoid robot. *IEEE Transactions on Industrial Electronics (TIE)*, 2008.

[3] Tomoya Sato, Sho Sakaino, Eijiro Ohashi, and Kouhei Ohnishi. Walking trajectory planning on stairs using virtual slope for biped robots. *IEEE Transactions on Industrial Electronics (TIE)*, 2011.

[4] EZ Moore, D Campbell, Felix Grimminger, and Martin Buehler. Reliable stair climbing in the simple hexapod'rhex'. In *IEEE International Conference on Robotics and Automation (ICRA)*, 2002.

[5] D Campbell and Martin Buehler. Stair descent in the simple hexapod'rhex'. In *IEEE International Conference on Robotics and Automation (ICRA)*, 2003.

[6] Ren C Luo, Ming Hsiao, and Tsung-Wei Lin. Erect wheel-legged stair climbing robot for indoor service applications. In *IEEE/RSJ International Conference on Intelligent Robots and Systems (IROS)*, 2013.

[7] Ren C Luo, Ming Hsiao, and Che-Wei Liu. Descending stairs locomotion and somatosensory control for an erect wheel-legged service robot. In *IEEE International Conference on Robotics and Automation (ICRA)*, 2014.

[8] J. Liu, Y. Wang, S. Ma, and B. Li. Analysis of stairs-climbing ability for a tracked reconfigurable modular robot. In *IEEE International Safety, Security and Rescue Robotics (SSRR)*, 2005.

[9] Nan Li, Shugen Ma, Bin Li, Minghui Wang, and Yuechao Wang. An online stair-climbing control method for a transformable tracked robot. In *IEEE International Conference on Robotics and Automation (ICRA)*, 2012.

[10] E Foo and Thanh Tung Le. Starcly robota novel compact stair climbing robot. In *International Conference on Mechanical and Electronics Engineering (ICMEE)*, 2010.

[11] Mark Yim, Sam Homans, and Kimon Roufas. Climbing with snake-like robots. In *IFAC workshop on mobile robot technology*, 2001.

[12] Yang, Yong, Huihuan Qian, Xinyu Wu, Guiyun Xu, and Yangsheng Xu. "A novel design of tri-star wheeled mobile robot for high obstacle climbing." In Intelligent Robots and Systems (IROS), 2012 IEEE/RSJ International Conference on, pp. 920-925. IEEE, 2012.

[13] T Estier, Y Crausaz, Bertrand Merminod, Michel Lauria, R Piguet, and Roland Siegwart. *An innovative space rover with extended climbing abilities*. ETH-Zurich, 2000.

[14] H Hong, D Kim, J Kim, J Oh, and HS Kim. A locomotive strategy for a stair-climbing mobile platform based on a new contact angle estimation. In *IEEE International Conference on Robotics and Automation (ICRA)*, 2013.

[15] Siravuru Avinash, Ankur Srivastava, Akshaya Purohit, Suril V Shah, and K Madhava Krishna. A compliant multi-module robot for climbing big step-like obstacles. In *IEEE International Conference on Robotics and Automation (ICRA), Hong Kong, China*, 2014.

[16] Arun Kumar Singh, Rahul Kumar Namdev, Vijay Eathakota, and K Madhava Krishna. A novel compliant rover for rough terrain mobility. In *IEEE/RSJ International Conference on Intelligent Robots and Systems (IROS)*, 2010.

[17] Ernst Neufert and Peter Neufert. *Architects' Data*. John Wiley & Sons, 2012.


## APPENDIX

The static equilibrium equations for the remaining phases (from subsection III A) of stair ascent are given below.

$$Phase-2\ Equations$$

$$\sum F_x = 0 \quad N_2 - F_1 - F_3 - F_4 = 0$$

$$\sum F_y = 0 \quad 3w_l + 8w_w - 2F_2 - 2N_1 - 2N_3 - 2N_4 = 0$$

$$\sum M_{J_1} = 0 \quad -2F_1(lsin\theta_1 - r) + 2N_1 lcos\theta_1 - w_l\left(\frac{l}{2}cos\theta_1 - csin\theta_1\right) - 2w_w lcos\theta_1 - \tau_1 = 0$$

$$\sum M_{J_2} = 0 \quad 2N_1(l+l_0)cos\theta_2 - 2F_1(l+l_0)sin\theta_2 - w_l\left(\frac{l}{2}cos\theta_2 - csin\theta_2\right) - 2w_w lcos\theta_2 - (w_l + 2w_w)(l+l_0)cos\theta_2 + 2F_2(lcos\theta_2 + r) + 2N_2 lsin\theta_2 - \tau_2 + \tau_1 = 0$$

$$\sum M_{W_4} = 0 \quad 2F_3 r + 2F_4 r + 2N_3 l - 2w_w l - w_l\left(\frac{l}{2}\right) - [2(2w_w + w_l) - 2F_2 - 2N_1](l+l_0) + \tau_2 = 0$$

$$Phase-3\ Equations$$

$$\sum F_x = 0 \quad F_1 + F_2 + F_4 - N_3 = 0$$

$$\sum F_y = 0 \quad 3w_l + 8w_w - 2F_3 - 2N_1 - 2N_2 - 2N_4 = 0$$

$$\sum M_{J_1} = 0 \quad 2N_1 lcos\theta_1 - 2w_w(lcos\theta_1) - 2F_1(lsin\theta_1 - r) - w_l\left(\frac{l}{2}cos\theta_1 - csin\theta_1\right) - \tau_1 = 0$$

$$\sum M_{J_2} = 0 \quad -2F_2(lsin\theta_2 - r) - 2F_1(l+l_0)sin\theta_2 - w_l\left(\frac{l}{2}cos\theta_2 - csin\theta_2\right) - (2w_w - 2N_2)lcos\theta_2 - \tau_2 + \tau_1 - (w_l + 2w_w - 2N_1)(l+l_0)cos\theta_2 = 0$$

$$\sum M_{W_4} = 0 \quad 2F_4 r + 2F_3(lcos\theta_3 + r) - 2w_w lcos\theta_3 - w_l\left(\frac{l}{2}cos\theta_3 - csin\theta_3\right) + 2N_3 lsin\theta_3 - (2F_1 + 2F_2)(l+l_0)sin\theta_3 + \tau_2 - [2(2w_w + w_l) - 2N_2 - 2N_1](l+l_0)cos\theta_3 = 0$$